Weather and Climate Extremes 53 (2026) 100924

Contents lists available at ScienceDirect

Weather and Climate Extremes

journal homepage: www.elsevier.com/locate/wace

Robustness and uncertainty in drought trend projections across dryland and non-dryland regions under greenhouse warming

Linchao Li [a,b], Qinsi He [b,c,*], Yu Shi [d], Puyu Feng [e], Limin Duan [b,c,**], Lijie Shi [f], Kai Ren [g], Ning Yao [h], Shang Chen [i], Ke Liu [j], Matthew Tom Harrison [j], Yi Li [h], De Li Liu [k,l], Alfredo Huete [c], Qiang Yu [g], Guijun Yang [m,n,***]

[a] College of Agronomy, Inner Mongolia Agricultural University, Hohhot, 010019, China
[b] College of Water Conservancy and Civil Engineering, Inner Mongolia Agricultural University, Hohhot, 010018, China
[c] School of Life Sciences, Faculty of Science, University of Technology Sydney, PO Box 123, Broadway, Sydney, NSW, 2007, Australia
[d] Institute of Carbon Neutrality, Sino-French Institute for Earth System Science, College of Urban and Environmental Sciences, Peking University, Beijing, 100871, China
[e] College of Land Science and Technology, China Agricultural University, Beijing, 100193, China
[f] College of Hydraulic Science and Engineering, Yangzhou University, Yangzhou, Jiangsu, 225009, China
[g] State Key Laboratory of Soil Erosion and Dryland Farming on the Loess Plateau, Institute of Soil and Water Conservation, Northwest A&F University, Yangling, Shaanxi, 712100, China
[h] College of Water Resources and Architectural Engineering, Northwest A&F University, Yangling, Shaanxi, 712100, China
[i] Jiangsu Key Laboratory of Agricultural Meteorology, Nanjing University of Information Science and Technology, Nanjing, China
[j] Tasmanian Institute of Agriculture, University of Tasmania, Newnham Drive, Launceston, Tasmania, 7248, Australia
[k] NSW Department of Primary Industries, Wagga Wagga Agricultural Institute, Wagga Wagga, NSW, 2650, Australia
[l] Climate Change Research Centre, University of New South Wales, Sydney, NSW, 2052, Australia
[m] College of Geological Engineering and Geomatics, Chang'an University, Xi'an, 710054, China
[n] Key Laboratory of Quantitative Remote Sensing in Agriculture of Ministry of Agriculture and Rural Affairs, Information Technology Research Center, Beijing Academy of Agriculture and Forestry Sciences, Beijing, 100097, China

ARTICLE INFO

Keywords:
Drought trends
Climate change
Global climate models
Greenhouse warming
Robustness and uncertainty
Cluster analysis

ABSTRACT

Droughts strongly affect ecosystems, hydrology, agrifood production, and their interactions, and understanding how drought trends may evolve under global warming is critical for climate adaptation. However, the robustness and sources of uncertainty in projected drought trends remain insufficiently quantified. Our results show that future drying signals differ systematically between dryland and non-dryland regions depending on the drought metric used. The Standardized Precipitation Evapotranspiration Index (SPEI) indicates stronger drying in drylands, where the area with significant decreases reaches 48-59% under SSP245 and 69-77% under SSP585, compared with 20-33% and 40-53% in non-drylands. In contrast, the Aridity Index (AI) indicates broader drying in non-dryland regions, where significantly affected areas reach 26-41% under SSP245 and 55-68% under SSP585, compared with 17-24% and 40-53% in drylands. Uncertainty is dominated by inter-model differences: GCMs explain 37.5% of the total variance, exceeding the contributions of emission scenario (18.4%) and drought-index choice (12.8%), indicating that model structural differences are the primary source of spread in projected drought trends. These findings show that future drought evolution depends strongly on both region type and drought metric, and they highlight the need to better constrain model-related uncertainty for more reliable drought-risk assessment under global warming.

1. Introduction

Droughts often detrimentally impact ecosystems (Shi et al., 2021; Zhang et al., 2021b), food production (Lobell et al., 2020; Mieno et al., 2024), and socioeconomic systems (Ercin et al., 2021; Naumann et al., 2021; Shahpari et al., 2021). For instance, the impacts of drought on

* Corresponding author. College of Water Conservancy and Civil Engineering, Inner Mongolia Agricultural University, Hohhot, 010018, China.
** Corresponding author. College of Water Conservancy and Civil Engineering, Inner Mongolia Agricultural University, Hohhot, 010018, China.
*** Corresponding author. College of Agronomy, Inner Mongolia Agricultural University, Hohhot, 010019, China.
E-mail addresses: qinsihe@outlook.com (Q. He), duanlimin820116@163.com (L. Duan), yanggj@nercita.org.cn (G. Yang).

https://doi.org/10.1016/j.wace.2026.100924
Received 6 January 2026; Received in revised form 10 June 2026; Accepted 10 June 2026
Available online 13 June 2026

gross primary production (GPP) are projected to triple by the end of the 21st century (2075-2099) compared with 1985-1999 (Xu et al., 2019). For food production, drought conditions significantly increase the risk of crop yield losses (Leng and Hall, 2019), and crop yields are shown to be more sensitive to drought events under climate change (Gampe et al., 2021; Lobell et al., 2020). Drought conditions are expected to increase due to greenhouse warming (Balting et al., 2021; Chiang et al., 2021), especially in drylands (Li et al., 2021), which also enhances the risk of drought occurring simultaneously in different regions (Singh et al., 2022). These increased drought risks could also lead to simultaneous yield shocks in different breadbaskets (Anderson et al., 2023; Gaupp et al., 2019). Developing robust drought trend projections and quantifying the source of uncertainties among different models is critical for developing more effective adaptation strategies under climate change.

Recently, some studies have projected drought trends using different Global Climate Models (GCMs) at regional scales (Shi et al., 2020; Yao et al., 2020) and global scales (Pokhrel et al., 2021; Zhang et al., 2022). For instance, arid regions such as northwestern China and Australia are likely to suffer more severe drought conditions (Chen et al., 2022; Zheng et al., 2024). Conversely, some humid regions, such as southeastern China (Chen et al., 2022) and Northern Europe (Christidis and Stott, 2021), are getting wetter. These conditions are often related to the "wet get wetter, dry get drier" (WWDD) mechanics (Allan et al., 2020; Held and Soden, 2006; Jin et al., 2023), which has been widely used to summarize global and regional wet-dry cycle trends (Liang and Zhang, 2022; Zaitchik et al., 2023). However, implications associated with the WWDD paradigm are very much subject to the selection of the drought index, the data source, the climate horizon, and the greenhouse gas emissions scenario (Xiong et al., 2022). Some regions show projections opposed to the WWDD mechanism under future climate change (Xiong et al., 2022). For example, drylands such as the Qinghai-Tibet Plateau are becoming wetter (Zhang et al., 2021a), while some humid regions, such as the Amazon, show significant drying trends for the 21st century (Parsons, 2020). Although many studies have projected drought trends under climate change, few have comprehensively identified the variability within and validity of the WWDD paradigm via comparison of drought indices using data from large GCM ensembles.

Drought conditions are mainly associated with precipitation and evapotranspiration and can be characterized using various drought indices (Guo et al., 2025; Xu et al., 2021). However, different indices reflect different drought characteristics due to their varied sensitivities to climate variables. For instance, the Standardized Precipitation Evapotranspiration Index (SPEI) reflects the balance between precipitation and potential evapotranspiration (PET) (Vicente-Serrano et al., 2010), which can be used to capture the effect of temperature and moisture on drought conditions (Shi et al., 2020; Yao et al., 2018). The Aridity Index (AI) provides insights into long-term dryness and a comprehensive picture of the water balance in different regions (Greve et al., 2019). Although the SPEI is easy to compare across different regions and times due to standardization, it can sometimes obscure the absolute levels of drought conditions. Using these two indices can provide a more complete perspective on drought trends under climate change.

Model ensemble configurations (e.g., model composition and size) impact drought projections due to the large output uncertainties across GCMs (Li et al., 2023a). For instance, GCMs with higher equilibrium climate sensitivity (ECS) often project stronger temperature increases (Galik, 2019), raising PET and producing more severe drought conditions. Consequently, different ensemble members can affect projections, and important information might be obscured when relying solely on ensemble means due to the considerable uncertainty within the large model pool (Li et al., 2023a; Sándor et al., 2023; Solazzo and Galmarini, 2015). Investigating model projections from different subsets of the ensemble can provide different perspectives, which have been applied in the projections of crop yields and wind-wave patterns (Li et al., 2023a; Morim et al., 2019). However, no such studies have been conducted to project drought trends.

Since the large uncertainties among different GCMs (John et al., 2022; Yazdandoost et al., 2021), identifying the main sources of uncertainty in drought projections is crucial for improving our understanding of drought evolution under climate change. Several studies have attributed uncertainty in such projections to variations in GCMs and emissions scenarios (Ji et al., 2024; Lu et al., 2019). Some studies have also identified the PET model used to calculate SPEI as an additional source of uncertainty, as projected drying in PET-based drought metrics may depend on the adopted PET formulation under greenhouse warming, particularly when temperature-driven approaches such as Thornthwaite are used (Frierson and Scheff, 2015; Shi et al., 2020). However, few studies have considered the uncertainty source from different drought indices. Moreover, previous studies have primarily focused on the uncertainty associated with drought intensity and frequency, rather than trends in drought over time and with the changing climate (Phelan et al., 2018). A systematic assessment of the sources of uncertainty implicit in drought trend projections will help bridge the gap in understanding long-term drought evolution under climate change.

Here, we project drought trends using the SPEI and AI using data from 36 GCMs and three shared socio-economic pathways (SSPs; SSP126, SSP245, and SSP585) from the Coupled Model Intercomparison Project (CMIP6). We make the trends of SPEI and AI comparable through standardized adjustments. This allows us to project drought trends from different perspectives. The objectives of this study are to (1) project drought characteristics using different indices and a multi-model ensemble under various scenarios, (2) reveal temporal and spatial patterns of drought and thus identify regions that are becoming drier or wetter, and (3) explore the sources of uncertainty in drought trend projections. This study can improve our understanding of drought evolution under climate change, which is important for developing water resource management practices.

2. Data and methods

2.1. Climate data

In this study, we employed 36 Global Climate Models (GCMs) from the Coupled Model Intercomparison Project (CMIP6) across three Shared Socioeconomic Pathways (SSPs): SSP126, SSP245, and SSP585 (Table S1). The SSP126, SSP245, and SSP585 represent a radiative forcing level projected at 2.6 W/m^2, 4.5 W/m^2, and 8.5 W/m^2, respectively (Liddicoat et al., 2021; O'Neill et al., 2016). These 36 GCMs include models with high equilibrium climate sensitivity (ECS), such as UKESM1-0-LL, IPSL-CM6A-LR, and HadGEM3-GC31-LL, medium ECS models like GFDL-CM4, EC-Earth3-Veg, and ACCESS-ESM1-5, and low ECS models such as INM-CM4-8 and INM-CM5-0 (Meehl et al., 2020). The historical period covered is 1930-2014, and the future projection period spans 2015-2099. This large ensemble can capture a broad range of climate conditions and provide a comprehensive insight into potential futures (Ruane and McDermid, 2017). To ensure compatibility with the spatial analysis, all 36 GCMs were resampled to a common 0.5° grid using bilinear interpolation. The multi-model median was then used as the primary ensemble statistic, because it reduces sensitivity to outlier model responses while preserving the spread of the ensemble. This unweighted ensemble approach provides a broad representation of CMIP6 uncertainty, but it does not constitute a bias-corrected or performance-weighted ensemble.

We compared the multi-GCM ensemble performance for temperature and precipitation against observational data from the 0.5° AgMERRA ("agricultural"-modified Modern-Era Retrospective Analysis for Research and Applications) gridded reanalysis product during 1980–2010. In general, temperature and precipitation showed broadly similar large-scale spatial patterns between the multi-model ensemble and AgMERRA observations, and the density plots also indicated similar

overall distributions (Fig. S1). We treat this comparison as a basic consistency check of the driving climate fields rather than as a formal validation of drought or aridity indices. Because this study focuses on relatively long-term drought trends and uncertainty partitioning rather than deterministic reconstruction of observed drought conditions, bias correction was not applied.

2.2. Drought index

2.2.1. Computation of SPEI

The SPEI is calculated by standardizing the difference between precipitation (P) and PET (Vicente-Serrano et al., 2010). PET was calculated using the Thornthwaite method (Thornthwaite, 1948). The SPEI has been widely used to project drought conditions at different time scales (Li et al., 2021; Yao et al., 2018), and has also been used to analyze the impacts on crop yields and ecosystems (Li et al., 2023b; Zhang et al., 2021b). In this study, we used the mean of negative annual SPEI values (SPEI $\leq$0) to characterize dry-anomaly intensity within a given period. Because SPEI is standardized around zero, values below zero indicate annual conditions that are drier than the local climatological normal. Therefore, SPEI $\leq$0 was used only as an anomaly-separation criterion to summarize the average magnitude of negative water-balance departures. It was not used as a categorical threshold for identifying drought events or estimating drought frequency. We acknowledge that stricter thresholds are more suitable for event-based drought classification, whereas our aim was to assess long-term drying tendencies by retaining all negative SPEI anomalies. The SPEI was calculated by the R package of 'SPEI' (https://cran.r-project.org/web/packages/SPEI/index.html).

2.2.2. Computation of Aridity Index

The Aridity Index (AI) is an effective method for estimating long-term climatic conditions, aiding in the identification of drylands and non-drylands. It is calculated as the ratio of annual precipitation to PET (Trabucco and Zomer, 2018). In this study, we use AI to identify the regions of dryland and non-dryland and analyze the drought evolution. Generally, both SPEI and AI are widely used for analyzing drought conditions. SPEI can be computed across different timescales and employs a standardization process that allows for comparisons across diverse intervals and regions. However, SPEI's reliance on a consistent historical baseline for standardization can complicate comparisons among different future scenarios. In contrast, AI does not depend on historical data for standardization, making it a more stable and absolute measure of dryness, suitable for consistent comparison across various climates and future conditions. Nonetheless, AI is less sensitive than SPEI to short-term temperature variability, primarily reflecting long-term drought conditions. By combining SPEI and AI, we comprehensively assess drought dynamics from both the relative deviations from historical conditions and absolute water balance perspectives. Since we mainly focus on the trends of SPEI and AI, bias correction of the GCMs is not necessary in this study. In this study, we use historical AI to identify regions of dryland and non-dryland. Since the AI may shift under climate warming, the dryland boundaries could expand or contract in future periods (Huang et al., 2015). However, to enable consistent comparisons of drought trends across scenarios and time periods, we use a fixed dryland and non-dryland classification based on the historical AI throughout the analysis.

In this study, we selected two complementary drought indices. The SPEI captures the balance between precipitation and potential evapotranspiration, reflecting relative deviations from historical conditions, while the AI represents the long-term water balance and absolute dryness level. To direct comparison with AI and to emphasize long-term drought evolution, SPEI was calculated from annual values and analyzed at the annual scale in this study. Using both indices on the same temporal basis reduced the influence of short-term variability and provided a more consistent framework for comparing SPEI- and AI-based trend projections. In addition, the absolute magnitudes of these two indices are not directly comparable; therefore, our analysis focuses primarily on their long-term trends rather than on absolute values. By combining these indices, we are able to characterize drought evolution from both relative and absolute perspectives. These differing constructions explain why the two indices may diverge in both magnitude and direction across regions and scenarios.

2.3. Sen's slope

The Sen's slope is a non-parametric approach used to analyze data trends, especially in time series analysis (Sen, 1968). This approach considers the median of possible pairwise slopes, effectively reducing the influence of extreme values. In this study, Sen's slope was used to quantify trends in climate variables (temperature and precipitation) and drought indices (SPEI and AI) during the historical (1930–2014) and future (2015–2099) periods. These two equal-length periods were defined for long-term trend comparison, particularly for comparing the spatial patterns of historical and future drought change, rather than as separate reference periods for SPEI standardization. This design enabled direct comparison of drought-trend magnitude and direction between historical and future climates while ensuring comparable Sen's slope estimates across periods of the same length. Each period spans 85 years, which helps identify stable long-term trends and reduces the influence of interannual variability. The calculation of Sen's slope is as follows:

$$\theta = Median\left(\frac{x_j - x_i}{j - i}\right) \quad (j > i) \tag{1}$$

Where x_j and x_i are values of annual temperature, precipitation, SPEI, and AI in i and j year, respectively. This study also analyzed the Sen's slope changes of SPEI and AI under a 30-year moving window. The moving-window analysis is intended to illustrate temporal trend evolution rather than statistical significance, which is assessed separately for fixed-period spatial trends. We chose a 30-year moving window as it is commonly used to detect climate trends and to minimize the influence of interannual variability. A shorter 10-year window could be more sensitive to internal variability and extreme events, leading to less stable trends. However, because SPEI values are standardized and not directly comparable in historical contexts, we used the ratio of SPEI to its standard deviation (SPEI/SD) to make adjustments for comparability.

2.4. Mann-Kendall (MK) test

The MK test analyzes the significance of time series trends (Kendall, 1975; Mann, 1945). In this study, we use the Z value from the MK test to analyze the SPEI and AI that significantly increase or decrease. A general expression for the MK test is calculated as follows:

$$S = \sum_{i=1}^{n-1} \sum_{j=i+1}^{n} \mathrm{sgn}(x_j - x_i) \tag{2}$$

Where sgn is calculated as:

$$\mathrm{sgn}(x) = \begin{cases} -1, for\ x < 0 \\ 0, for\ x = 0 \\ 1, for\ x > 0 \end{cases} \tag{3}$$

The Z value is calculated as follows:

$$Z = \begin{cases} \dfrac{S-1}{\sqrt{Var(S)}} & if \quad S > 0 \\ 0 \quad if \quad S = 0 \\ \dfrac{S+1}{\sqrt{Var(S)}} & if \quad S > 0 \end{cases} \tag{4}$$

Z was used to identify the significant trends in SPEI and AI. A $Z > 1.96$ indicates a statistically significant increase. Conversely, a $Z < -1.96$

indicates a statistically significant decrease.

2.5. Cluster analysis

We used an agglomerative-hierarchical clustering approach to provide drought trend projections from different ensemble members. Our study uses the Manhattan distance (D) to compute the distances between different drought trend projections among 36 GCMs (Borg and Groenen, 2005; Willett, 1988). This method used drought trend results at each grid location and was applied without pre-selection. It allowed us to identify GCMs with high similarity in spatial patterns of drought trends and reveal drought projections from different ensemble members. This approach has been applied to crop yield changes (Li et al., 2023a), warming (Brunner et al., 2020), and wind-wave climate projections (Brunner et al., 2020) to reveal results from different ensemble members as well as quantifying their independent weights. We applied a single hierarchical clustering approach using Manhattan distance and complete linkage to group GCMs. The optimal number of clusters was determined using the Gap statistic (B = 100), evaluated across k = 2–10 within the same clustering framework. Based on this diagnostic, the optimal number of clusters was k = 3 for SPEI and k = 2 for AI. To facilitate direct comparison between SPEI- and AI-based groupings, we additionally present AI clustering results using k = 3 alongside the optimal k = 2 solution. All GCMs were analyzed on the same regular grid, and grid cells were equally weighted when characterizing spatial drought trend patterns for clustering. In this study, we applied cluster analysis for drought trends to identify differences and similarities across the 36 GCMs, providing new insights into drought evolution projections and guiding model selection for further analysis or policy-making. Cluster analysis focused on SSP585 because drought-trend signals were strongest and most spatially coherent under this scenario, allowing model differences to be more clearly distinguished.

2.6. Consistent across models

In this study, we quantified the consistency of projected drought trends using an inter-model agreement metric. For each grid cell, we first computed Sen's slope for each CMIP6 model. The sign of the multi-model median Sen's slope was then used as the reference trend direction (positive indicating a wetting tendency and negative indicating a drying tendency). Inter-model agreement was defined as the percentage of models whose Sen's slope sign matched the reference direction, calculated as:

$$Agreement\ (\%) = \frac{N_{agree}}{N_{total}} \times 100 \tag{5}$$

Where, N_{agree} is the number of models with the same trend as the multi-model median, and N_{total} is the total number of models.

2.7. Uncertainty analysis

We used a three-factor analysis of variance (ANOVA) to quantify the dominant sources of uncertainty in drought trends under future climate change. Since SPEI and AI differ in units and variability, we normalized each index by its temporal standard deviation (SD) to improve comparability in trend and uncertainty analyses. Specifically, SD was calculated at each grid cell over the analysis period, and we used SPEI/SD and AI/SD as dimensionless standardized metrics in the ANOVA-based uncertainty decomposition. The formula of ANOVA is as follows:

$$SS = SS_{Index} + SS_{GCM} + SS_{SSP} + SS_{GCM\times Index} + SS_{SSP\times Index} + SS_{GCM\times SSP} + SS_{GCM\times SSP\times Index} \tag{6}$$

Where SS_{Index} SS_{GCM} SS_{SSP} are the uncertainty sources from GCM, drought index, and SSP. $SS_{GCM\times Index}$ + $SS_{SSP\times Index}$ + $SS_{GCM\times SSP}$ + $SS_{GCM\times SSP\times Index}$ represent their interaction influence. The interaction terms capture non-additive effects, where the impact of one factor depends on the level of another index.

3. Results

3.1. Projected climate change

Temperature and precipitation showed distinct trend patterns across scenarios (Fig. 1a). During the historical period (1930–2014), precipitation trends were generally weak, with slight decreases in southern Asia, Brazil, and southern Africa and slight increases in northern Africa. Under SSP126, precipitation changed little overall, with slight increases across much of the Northern Hemisphere and slight decreases in parts of Africa and Australia. Under SSP585, precipitation increased more strongly across most regions, except for parts of northern Africa, South Africa, and northern South America, which show a decrease. Temperature trends under SSP126 showed little change compared to the historical period, whereas under SSP585, there is a substantial increase in temperature (Fig. 1a). Although precipitation increases with greenhouse warming, the higher temperatures likely increase PET, accelerating drought conditions. The spatial patterns of temperature and precipitation trends are shown in Fig. S2. In this study, drylands were defined as areas with AI < 0.65 (Fig. S3). Although the precipitation shows a larger magnitude increase in non-dryland than in dryland, both areas have a similar relative increase under three scenarios (Fig. 1b). Incremental gains in temperature were similar in dryland and non-dryland regions, although historical temperatures in dryland regions were higher.

3.2. Temporal variation in drought indices

The time series of SPEI and the relative change in AI from 1930 to 2099 showed distinct changes in drought characteristics across scenarios (Fig. 2). SPEI was presented as a continuous annual time series over the full study period (1930–2099). SPEI is shown as a continuous annual series over the full analysis period rather than being standardized separately within sub-periods. Historical SPEI values were generally higher than those under future scenarios, especially SSP585. Overall, both SPEI and AI decreased under climate change, with the strongest decline under SSP585. In dryland regions, SPEI showed a larger decrease, dropping from approximately 0.39 in 1930 to around −0.33 under SSP126 and -1.1 under SSP585. SSP245 falls between SSP126 and SSP585. SSP126 shows little change or a slight increase after 2050. In non-dryland regions, SPEI showed a smaller decline, decreasing from around 0.15 in 1930 to about −0.05 under SSP126 and -0.55 under SSP585. Although SPEI shows a larger decrease in magnitude in drylands, AI indicates a more substantial decrease in non-dryland regions, with reductions of 21% in non-drylands and 17% in drylands under SSP585. This indicates that different indices can reflect different levels of drought change.

The SSP585 scenario shows a stronger increase in drought intensity compared to SSP126 and SSP245 (Fig. S4) for the future period, especially in the Middle East, northern Africa, and parts of South America. Some regions, such as parts of North America and Asia, show a slight decrease in drought intensity. For AI, there is a substantial decrease across many regions, particularly in South America, southern Africa, and parts of Asia, indicating a significant increase in drought conditions (Fig. S5). Generally, drought conditions increase with higher forcing scenarios, indicating that greenhouse warming exacerbates drought severity.

3.3. Drought trend projection under future scenarios

SPEI and AI showed broadly similar drying tendencies in many regions, but with region-specific differences in trend magnitude and direction under future climate change (Fig. 3 and Fig. S6). The SPEI trend showed limited change during the historical period and under SSP126

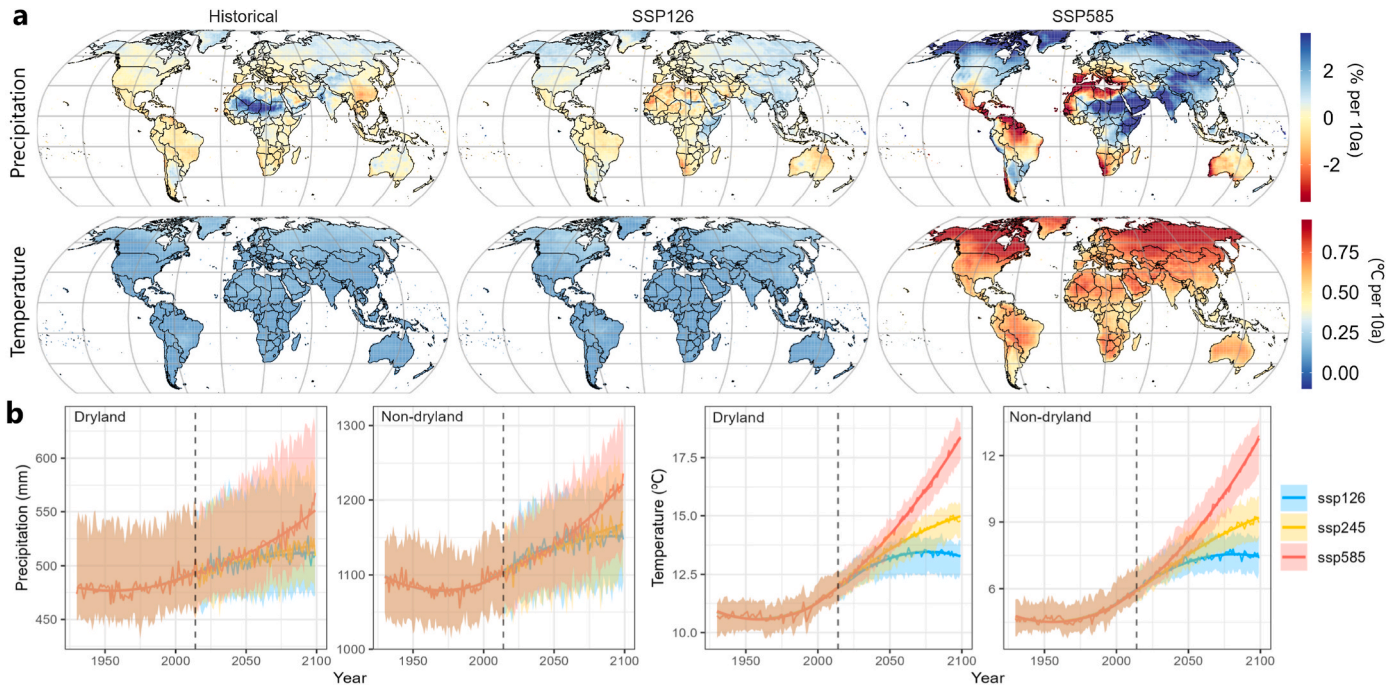

Fig. 1. Precipitation and temperature trends during historical (1930–2014) and future (2015–2099) climate periods. a, Spatial patterns of temperature and precipitation trends in historical and future periods, calculated using Sen's slope based on the multi-model median (36 GCMs) under SSP126 and SSP585 scenarios. **b**, Time series in multi-model ensemble median values of precipitation and temperature from 1930 to 2099 under SSP126, SSP245, and SSP585 scenarios for dryland and non-dryland regions. Shaded areas represent the 25th and 75th percentiles. The black dashed lines divide the historical and future periods.

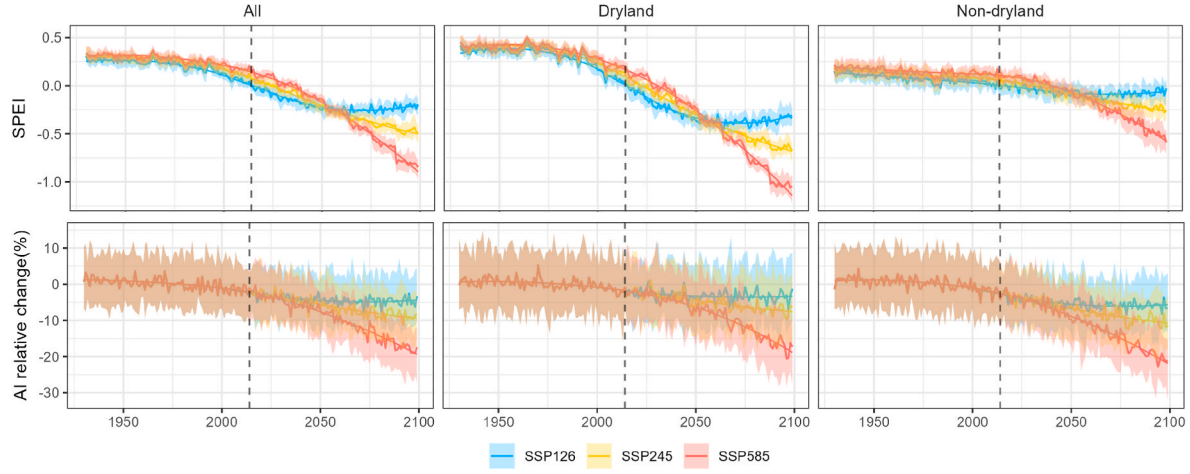

Fig. 2. Time series of multi-model median area-mean SPEI and relative change in AI from 1930 to 2099 for dryland, non-dryland, and all regions under SSP126, SSP245, and SSP585. Shaded areas indicate the 25th and 75th percentiles across the 36 GCMs. Black dashed lines separate the historical (1930–2014) and future (2015–2099) periods. SPEI is shown as a continuous annual series over the full analysis period.

(Fig. 3a). Negative trends occurred in northern Africa, which are even more pronounced during the historical period than those in the future period under SSP126. However, the SPEI trends under SSP245 and SSP585 show more pronounced negative trends in most regions, particularly in Africa, the Middle East, and South America, with the most severe changes observed under SSP585. Approximately 46% and 65% of areas exhibit SPEI trends lower than −0.1 per decade under SSP245 and SSP585, respectively, compared to only around 15% of areas showing trends lower than −0.1 under the historical period and SSP126 (Fig. 3c). For AI trend projections, the AI trends are around 0 during the historical period and under the SSP126 scenario. Under SSP245 and SSP585, although AI shows decreasing trends in most regions, the spatial patterns are different in some regions compared with the SPEI trends (Fig. S6).

The two indices generally agreed in projecting drying across parts of Africa and South America and wetting over the Tibetan Plateau, whereas clearer contrasts occurred in northern Africa and the Middle East, where SPEI showed stronger drying, and in parts of North America and Europe, where AI indicated drying but SPEI showed weak wetting tendencies. Overall, SPEI is more sensitive to climate change, especially in dryland regions, while AI indicates broader regions with increased drought conditions under SSP585, particularly in non-dryland regions. In drylands, even modest increases in PET substantially reduce the water balance (P-PET), resulting in stronger negative SPEI trends. In contrast, changes in AI are smaller when both precipitation and PET remain low. In non-drylands, where precipitation is generally higher, insufficient compensation for rising PET lowers the P/PET ratio, leading to stronger

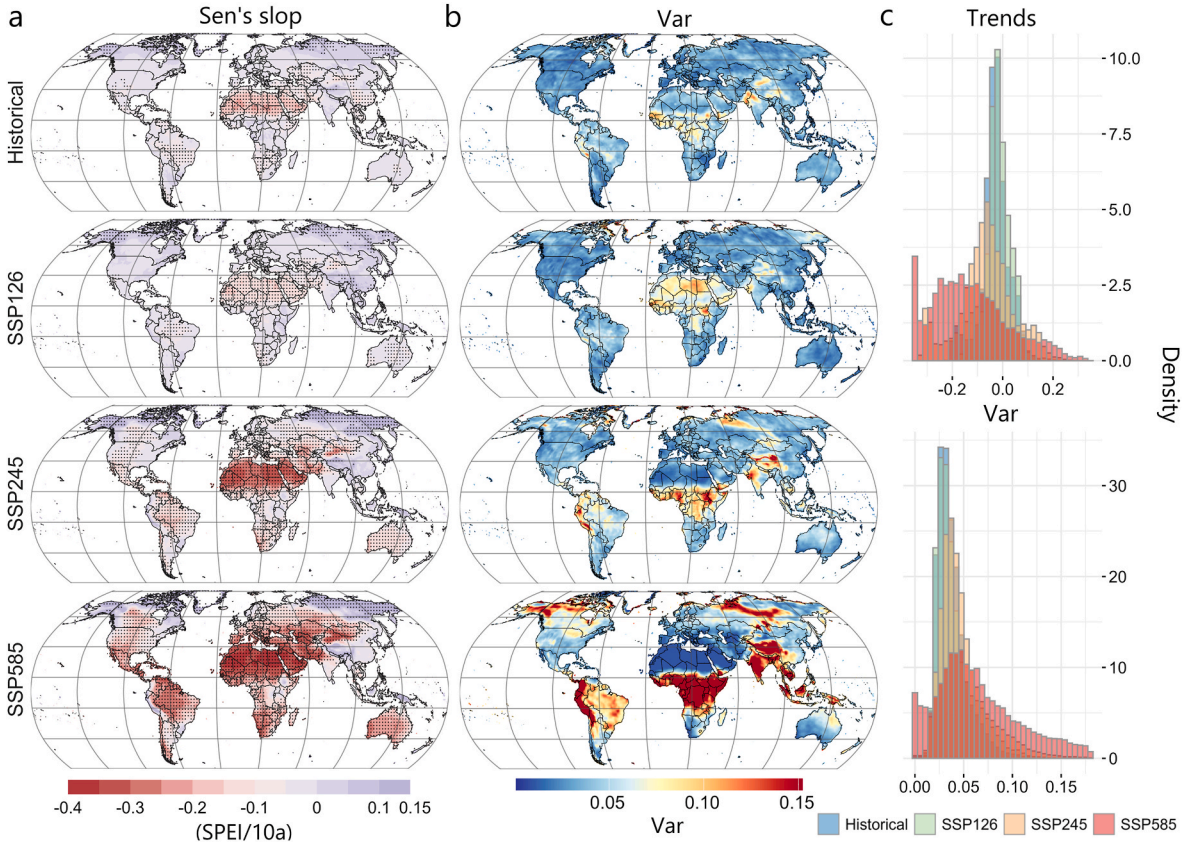

Fig. 3. Spatial patterns of SPEI trends in the historical period (1930–2014) and future period (2015–2099) under SSP126, SSP245, and SSP585. a, Multi-model median Sen's slope of SPEI among 36 GCMs, representing SPEI trends (per 10 years) under different scenarios. Stippled grid cells indicate robust trend signals, defined as locations where at least 80% of CMIP6 models agree on the sign of the multi-model median trend. b, Inter-model variance of Sen's slope among the 36 GCMs, representing the spread of projected trends. c, Density distributions of trend values and inter-model variance during the historical period and the three future scenarios.

AI declines.

The inter-model variance of SPEI and AI Sen's slopes among the 36 GCMs represents the spread of projected drought trends under each scenario (Fig. 3b and Fig. S6b), whereas robust trend signals are indicated directly on the main trend maps by stippling. Stippled grid cells denote locations where at least 80% of CMIP6 models agree on the sign of the multi-model median Sen's slope. Robust drying signals were widespread under SSP126 and SSP245 in many regions and became more spatially extensive under SSP585, particularly for SPEI. In contrast, several regions, including parts of South America, the Tibetan Plateau, Central Africa, and parts of North America, showed relatively high inter-model variance under SSP585, indicating greater spread in projected trend magnitude among models. By comparison, lower variance together with widespread stippling in Europe and Australia indicated more consistent projections of drying for both indices. The spatial mismatch in inter-model variance between SPEI and AI is mainly related to their different index constructions. SPEI is based on standardized anomalies of climatic water balance, whereas AI is based on the ratio between precipitation and PET. Therefore, model differences in precipitation and PET can be amplified in different regions by the two indices. In drylands, uncertainty in PET-driven water-balance changes can lead to larger SPEI spread, while in humid or transitional regions, AI is more sensitive to model differences in whether precipitation changes compensate for increasing PET. The full spatial patterns of inter-model agreement are shown in Fig. S7–S9. Agreement generally exceeded 80% across most regions, particularly for SPEI and in dryland regions, and tended to increase from SSP126 to SSP585, indicating greater model consistency in projected drought changes under stronger greenhouse warming.

Thirty-year moving-window trends showed substantial scenario-dependent changes in both SPEI and AI (Fig. 4a). We find that during 1930-2014, the SPEI Sen's slope decreased over time. There is a slight increase after 2020 under SSP126 and after 2030 under SSP245. For SSP585, drought trends show a strong decrease in dryland regions but change relatively little after 2050 in non-dryland regions. The trend change patterns of AI are similar to those of SPEI, but AI shows a lower magnitude. The percentage of area showing significant decreases increased markedly across scenarios for both SPEI and AI (Fig. 4b; Fig. S10). We find that around 22-34%, 13-34%, 48-59%, and 69-77% of dryland regions, and around 11-18%, 5.5-12%, 20-33%, and 40-53% of non-dryland regions shows a significant decrease in SPEI under the Historical, SSP126, SSP245, and SSP585 scenarios, respectively. For AI, there are around 6.3-10%, 5.1-9.5%, 17-24%, and 40-53% for dryland regions, and 11-19%, 5.6-13%, 26-41%, and 55-68% for non-dryland regions. Regions with significant increases in SPEI and AI were less extensive than regions with significant decreases (Fig. 4 and S6). Statistically significant hotspots of increasing drought risk broadly matched the trend patterns shown in Fig. 4 and Fig. S6 (Fig. S11–S12). Overall, regions showing increased drought risk in the trend analyses (Fig. 4 and Fig. S6) also tend to exhibit statistically significant changes, highlighting robust “hotspots” of increasing drought risk. Comparing SPEI and AI, we find that the two indices show broadly similar spatial patterns in trend direction over most regions, but differ in the significance of those trends, particularly under SSP126 and SSP245. Specifically, significantly increasing drought risk is projected more extensively for SPEI than for AI. This discrepancy likely reflects differences in index construction. Generally, more areas show significant decreases in SPEI in dryland regions, while more areas show significant decreases in AI in non-

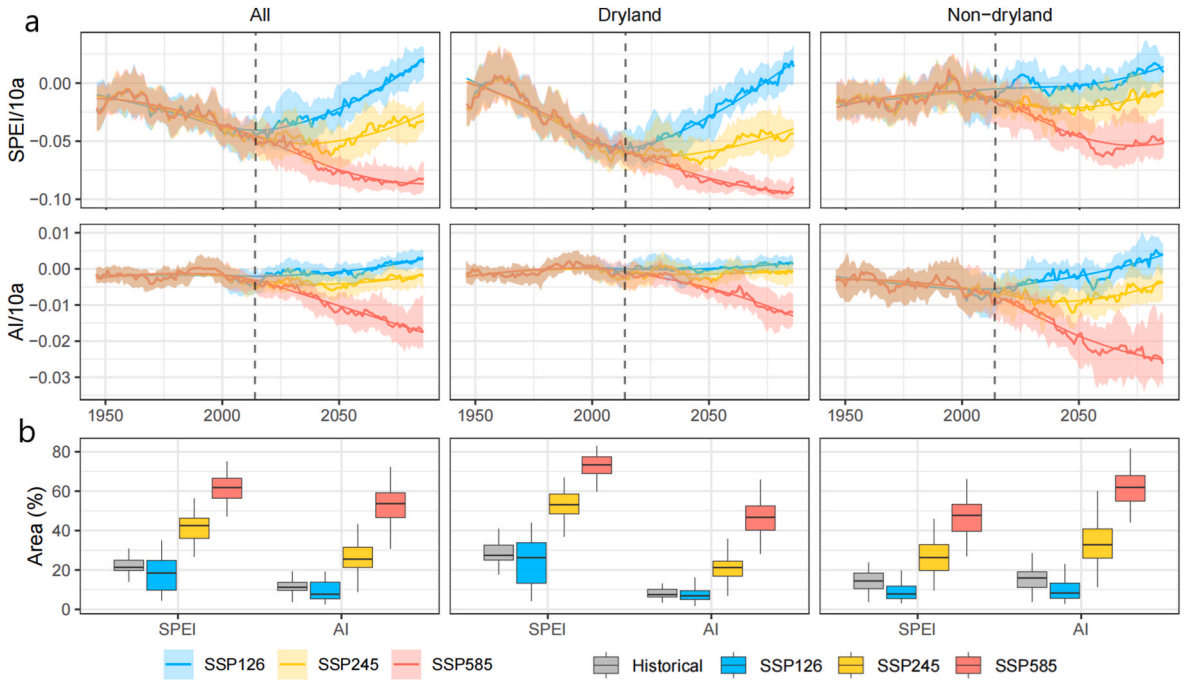

Fig. 4. Drought trends using a 30-year moving window under SSP126, SSP245, and SSP585. a, The SPEI and AI trends quantified by Sen's slope over a 30-year moving window for all regions, dryland, and non-dryland areas. In each panel, the thin solid line shows the median trend across the 36 GCMs for each window, and the thick solid line shows the smoothed median trend. **b**, The percentage of areas with a significant decrease ($Z < -1.96$) tested by the MK test under historical, SSP126, SSP245, and SSP585. Box boundaries indicate the 25th and 75th percentiles across 36 GCMs.

dryland regions.

Since there are still large uncertainties among different GCMs, ensemble members largely impact the model projections (Li et al., 2023a). Our results indicate that, among the various scenarios, drought trends under SSP585 exhibit considerable variance (Fig. 3 and Fig. S6). To fully capture the drought trends from different ensemble members, we applied cluster analysis to the drought trend (SPEI and AI) projections under SSP585. We find that ensemble members greatly impact drought trend projections (Fig. 5 and Fig. S13), particularly in regions with high variances. For example, cluster 3 (cluster 2 for Fig. S14) projects significant decreases in AI, especially in parts of South America, Africa, Europe, and southern Asia, whereas cluster 1 does not show such pronounced trends (Figs. S13–S14). Similarly, for SPEI, different clusters exhibit varying trends in regions with high variance among the 36 GCMs (Fig. 5). The cluster analysis indicates that the ensemble is not homogeneous but instead organizes into distinct groups of GCMs with similar drought signals. This suggests that part of the inter-model uncertainty quantified in the ANOVA arises from these structured differences. This analysis provides an interpretive link between the raw spread of GCM projections.

3.4. *The uncertainty analysis*

The dominant sources of uncertainty varied among regions and among the three main factors considered (GCM, SSP, and drought index) (Fig. 6). The GCM was the dominant source of uncertainty regarding drought trend projection in the Tibetan Plateau, Central Africa, Europe, and Southern South America. The drought index was the main source of uncertainty in Northern Africa, the Middle East, Northwest China, and Eastern Canada. In Southern Europe, the northern part of South America, and parts of Africa, SSP was the dominant source of uncertainty. Generally, the GCM contributed 44.2%, 31.6%, and 37.5% of

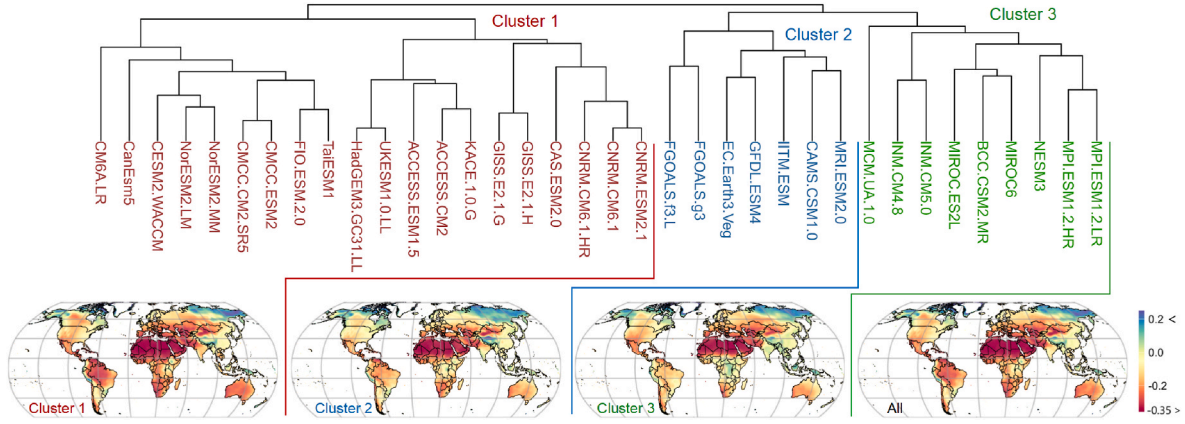

Fig. 5. Hierarchical clustering of CMIP6 GCMs based on gridded SPEI trend patterns for 2015–2099 under SSP585. The top panel shows the dendrogram derived using Manhattan distance and complete linkage, with models grouped into three clusters. The bottom panel maps the multi-model median SPEI trends for each cluster, illustrating distinct spatial patterns of projected drought trends across model subsets.

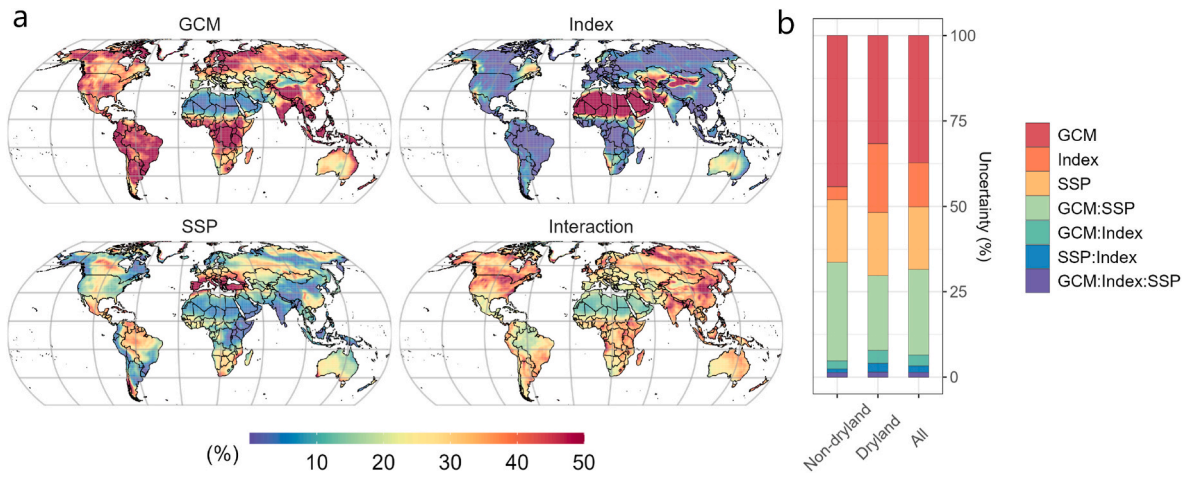

Fig. 6. The relative contribution of different sources of uncertainty in projecting drought trends under various GCMs, SSPs, and indices. Each drought index was standardized for comparability by its ratio to the standard deviation. **a**, Spatial uncertainty distribution attributed to GCM, SSP, Index, and their interactions. The "Interaction" category represents the sum of GCM, SSP, and Index interactions, including GCM-SSP, GCM-Index, SSP-Index, and GCM-Index-SSP interactions. **b**, Average contribution of each source of uncertainty and their interactions in non-dryland, dryland, and all regions.

uncertainty in non-dryland, dryland, and all regions, respectively. The proportion of uncertainty from the drought index exhibited a significant difference between non-dryland, dryland, and all regions, accounting for 3.8%, 20.1%, and 12.8%, respectively. The SSP contributed 18.2%, 18.6%, and 18.4% of uncertainty in non-dryland, dryland, and all regions, showing similar contributions for dryland and non-dryland regions.

4. Discussion

4.1. Drought evolution under climate change

Our results show that the SPEI shows a large reduction in dryland in the future under SSP245 and SSP585 (Fig. 2), indicating a pronounced increase in drying risk in these regions. At the large scale, this pattern is broadly consistent with the wet-gets-wetter, dry-gets-drier (WWDD) paradigm, because warming tends to increase atmospheric evaporative demand and amplify moisture deficits in already dry regions, even where moisture transport and precipitation may increase elsewhere (Chou et al., 2009; Zhou et al., 2022). However, the WWDD framework does not fully explain the regional patterns shown in Fig. 3 and Fig. S6. For instance, both SPEI and AI project a wetting trend in the Tibetan Plateau (Fig. 3 and Fig. S6). This wetting is more likely associated with circulation-related increases in moisture transport and enhanced precipitation under warming, including changes in the subtropical westerly jet and monsoonal influences (Zhang et al., 2020). By contrast, parts of humid tropical regions, including the Amazon, show a drying trend under greenhouse warming, especially under SSP585 (Fig. 3 and Fig. S6). This projected drying is more directly interpreted as reflecting the combined effect of increased atmospheric evaporative demand and projected precipitation changes under warming. This interpretation is consistent with CMIP6-based analyses showing that, in some models, although increasing temperature and drying can offset the positive effect of CO_2 fertilization and trigger localized Amazon dieback (Parry et al., 2022), these processes were not explicitly diagnosed in this study. In addition, large-scale climate variability associated with ENSO may further modulate drought risk in the Amazon (Singh et al., 2022), while deforestation may further reduce forest resilience in the region (Flores et al., 2024). Overall, these results indicate that, although WWDD captures broad large-scale tendencies, regional drought evolution is more complex and depends on circulation changes and the balance between precipitation and atmospheric evaporative demand, particularly in humid or transitional regions where the sign of change may differ from the large-scale expectation (Greve and Seneviratne, 2015).

4.2. Model selection impact on drought trend projection

We showed that GCM selection can significantly influence drought trend projections (Fig. 5 and Fig. S8). Climate change projections are basically classified as relatively cool-wet, cool-dry, middle, hot-wet, and hot-dry over the full GCM range (Ruane and McDermid, 2017). This classification potentially helps in selecting suitable subsets that effectively reflect the full range of GCMs (McSweeney and Jones, 2016; Ruane and McDermid, 2017). However, because different GCMs project different climate conditions, the multi-model ensemble may mask model-specific process differences, as opposing responses across models can partially cancel out. Our community ensemble incorporates different potential ensemble members that can provide a comprehensive overview of drought trend projections. Each cluster, therefore, represents a different mode of drought evolution, highlighting systematic inter-model differences that can be obscured by the multi-model mean (Li et al., 2023a; Morim et al., 2019). In addition, while the multi-model ensemble provides a useful approach for projection, our results indicate that it may reflect an average across fundamentally different drought-evolution pathways. Consequently, relying on the ensemble mean alone can mask regionally important contrasts in drought-risk trajectories and may result in a redundant representation of ensemble projections (Solazzo and Galmarini, 2015). The cluster-based framework offers a structured way to interpret projection uncertainty by identifying regions where model groups consistently indicate increasing drought risk versus regions where signals diverge across clusters. For instance, policymakers can select representative models from each cluster to reduce computational demands. In addition, the GCMs with high ECS tend to project stronger drought trends (Fig. 5 and Fig. S13). ECS refers to the equilibrium temperature increase resulting from a doubling of CO_2 (IPCC and Intergovernmental Panel on Climate, 2023; Meehl et al., 2020). Higher ECS models generally predict higher temperatures and increased PET, leading to more severe drought conditions. For example, the GCMs in Cluster 1 of the SPEI trend projections (Fig. 5) and Cluster 3 of the AI trend projections (Fig. S13), which include a higher proportion of high-ECS models (Hausfather et al., 2022), tend to project stronger increases in drought severity. Under these assumptions, more international efforts are needed to reduce net greenhouse gas emissions to achieve sustainable development (Scafetta, 2022). Our results show that different GCMs form clusters with internally consistent drought projections but divergent signals across groups. Such results

indicated that the future drought may have different potential conditions within the ensemble. Although this cluster analysis does not reduce the overall uncertainty, it clarifies its origin by distinguishing systematic inter-modal differences.

4.3. The source of uncertainty in drought trend projections

The drought projections are robust in some regions, such as the Amazon, Mediterranean, and Australia, similar to previous studies (Ukkola et al., 2020). However, there are still some regions that do not exhibit great agreement in drought trend projections (Fig. 3). GCMs are the main source of uncertainties in drought trend projections for the Tibetan Plateau, Central Africa, Europe, and Southern South America. The GCM-induced uncertainty is largely related to the precipitation projections, which are influenced by changes in circulation and can be partly explained by model-dependent responses to uniform sea surface temperature warming (Chen et al., 2020). Such processes are especially complex in regions like the Tibetan Plateau (Huang et al., 2023). In addition, GCMs contribute more uncertainty in dryland regions, perhaps because drought conditions in these regions are highly sensitive to precipitation variability, which varies among different GCMs.

Different scenarios represent the different levels of greenhouse gas emission (Gurney et al., 2022), which impact global warming and PET. Our results showed that the SSP is the main source of uncertainty in the Mediterranean, the northern part of South America, and parts of Africa (Fig. 6). In the northern part of South America and parts of Africa, monsoon systems largely influence regional precipitation patterns, which are sensitive to greenhouse warming (Almazroui et al., 2021; Nicholson, 2013). The Mediterranean climate is sensitive to atmospheric circulation patterns (such as the North Atlantic Oscillation), which are associated with moisture and vary among different SSPs (Fernandez-Alvarez et al., 2023; Rivosecchi et al., 2024). SSP forcing trajectories increase PET via warming and alter precipitation through circulation and moisture-transport changes. Models spread reflects differences in ECS, hydrological sensitivity, and land-atmosphere coupling, which propagate into drought indices.

In some regions, such as Northern Africa, the Middle East, and Eastern Canada the drought index is the main source of uncertainty. Generally, regions where drought indices dominate uncertainty are primarily located within drylands, indicating that the selection of drought indices should be treated with caution to accurately characterize drought conditions in such regions. The SPEI is more sensitive to temperature and can better capture the drought trends in extreme dryness regions like Northern Africa and the Middle East. In contrast, AI may not reflect significant trends in such regions. AI is likely more sensitive to the balance between land water supply and atmospheric water demand (Greve et al., 2014). In humid regions such as Eastern Canada, large variations in precipitation due to atmospheric circulation (Chartrand and Pausata, 2020) could be effectively captured by AI. This can also explain why non-dryland areas show a significant decrease in AI (Fig. 4).

4.4. Implications for food security and sustainable agriculture

Our study reveals drought trends under future climate change, which is important for agricultural production. Leng and Hall (2019) projected the risk of crop yield losses (maize, wheat, rice, and soybean) under drought events in different sub-regions globally. Some regions are likely to experience more severe drought conditions, while others may become wetter. Understanding future drought trends can provide detailed guidance for developing adaptation management practices for drought events. Recent studies find that drought events can occur simultaneously in multiple regions, increasing the risk of concurrent yield losses in different breadbaskets (Gaupp et al., 2019; Singh et al., 2022). In this study, we identified regions with strong drying trends and high agreement among different GCMs, including key breadbaskets, highlighting the need for increasing attention to water management in these regions. For instance, in regions such as the U.S. Midwest and the Australian wheat belt, which are highly dependent on rainfed systems, our results show an increasing drought risk with strong consistency across GCMs (Fig. 3). Therefore, timely adaptation measures such as adjusting sowing dates (Minoli et al., 2022), selecting suitable varieties (Zabel et al., 2021), or switching crops (Chakraborti et al., 2023) could help sustain yields in these areas and improve the climate resilience of food systems.

In this study, we find a significant increase in drought conditions due to greenhouse warming. Several management practices are being applied for greenhouse gas (GHG) mitigation (He et al., 2022; Xie et al., 2023; Xu et al., 2024) to reduce global warming. For example, retaining residues can mitigate GHG emissions by soil organic carbon sequestration (He et al., 2022); using large-scale bioenergy with carbon capture and storage is also an effective negative-emission technology for reducing GHGs (Xu et al., 2022). In addition, optimizing nitrogen management can reduce nitrous oxide emissions and contribute to sustainable agriculture (Yao et al., 2024). Moving forward, more efforts are urgently needed to mitigate GHG emissions and reduce the risk of greenhouse warming-induced drought events in the future.

4.5. Limitations and future work

There are several limitations in this study. First, since both SPEI and AI consider PET, it could be influenced by different PET models (Peng et al., 2017). For example, Yao et al. (2019) found that different PET models affect the minimum SPEI and frequency values, leading to large differences in arid regions. Shi et al. (2020) quantified the source of uncertainty in drought projections, considering different PET models in southeastern Australia. In addition, PET in this study was estimated using the temperature-based Thornthwaite method, which has been reported to potentially overestimate drought trends under climate warming (Sheffield et al., 2012). However, our study does not consider different PET models in drought trend projections. More physically based approaches, such as the FAO56 Penman-Monteith equation, are widely used (Allen et al., 1998; Xiang et al., 2020), but were not adopted here because the meteorological variables required by this method were not consistently available across the full GCM ensemble. Consequently, the PET-method uncertainty was not included in our uncertainty decomposition. The reported contributions of GCMs, SSPs, drought indices, and their interactions should therefore be interpreted as conditional on the adopted Thornthwaite PET formulation, rather than as a complete accounting of all uncertainty sources. Although we compared the large-scale spatial patterns of temperature and precipitation between AgMERRA and the multi-model ensemble, we did not perform a full observational validation of SPEI and AI or quantify ensemble bias metrics. Therefore, the results should be interpreted primarily in terms of relative trend patterns and uncertainty partitioning, rather than as an exact reconstruction of observed drought magnitude. Second, some drought indices, including the standard precipitation index (SPI), evaporative demand drought index (EDDI), and Palmer drought severity index (PDSI), could also capture drought characteristics from different perspectives. In this study, we only considered two indices, and more indices could be considered in further work. In addition, the uncertainty decomposition uses an ANOVA approach, but its assumptions (normality, homoscedasticity, and independence) were not formally tested. Although we SD-normalized the indices (e.g., SPEI/SD and AI/SD) to ensure comparability and reduce scale effects, remaining distributional differences may affect the quantitative contributions. Third, climate drivers such as ENSO, NAO, Indian Ocean Dipole (IOD), and Southern Annular Mode (SAM) play different roles in regional climate conditions (Jones et al., 1997; McPhaden et al., 2006; Saji and Yamagata, 2003; Stephenson et al., 2006). For instance, the NAO strongly influences the winter precipitation in Europe (McKenna and Maycock, 2021). ENSO is particularly important in influencing the availability of water in the Southern Hemisphere (Zhang et al., 2023).

Therefore, projecting drought evolution under greenhouse warming by incorporating different climate drivers can improve our understanding of drought risk changes under atmospheric circulation. Our future work will explore the potential changes in the non-linear relationships between drought indices and climate drivers (e.g., NAO, ENSO, and IOD) under greenhouse warming.

5. Conclusions

Our study comprehensively explored the uncertainty in drought trend projections under greenhouse warming. We projected drought trends using multiple drought indices and identified key sources of uncertainty across GCMs, SSPs, drought indices, and their interactions. We had four key insights: (1) SPEI shows larger-magnitude drying trends in drylands, especially under SSP245 and SSP585, while AI shows a more substantial decrease in non-dryland regions. (2) Higher GHG emission scenarios show stronger drought trends than lower GHG emission scenarios in most regions. (3) Different GCM members can substantially influence projected drought trends, resulting in divergent regional drought-change signals across models. (4) Overall, GCM-related differences represent a dominant source of projection uncertainty across most regions and drought metrics, while the leading uncertainty component can vary by region and metric. The drought index contributes more to uncertainty in dryland regions. SSPs contribute similarly to the overall uncertainty in both dryland and non-dryland regions. This study presents a comprehensive framework for projecting drought characteristics, providing critical insights for managing agriculture and ecosystems. Future research should focus on the relationship between drought events and climate drivers (e.g., ENSO and IOD) under greenhouse warming to enhance the reliability of drought trend projections and inform adaptation strategies.

Data

The CMIP6 data used in this study to project drought trends are available at: https://esgf-node.llnl.gov/projects/cmip6/.

CRediT authorship contribution statement

Linchao Li: Conceptualization, Data curation, Formal analysis, Investigation, Methodology, Software, Visualization, Writing – original draft. **Qinsi He:** Conceptualization, Data curation, Formal analysis, Funding acquisition, Methodology, Resources, Supervision, Writing – original draft, Writing – review & editing. **Yu Shi:** Conceptualization, Investigation, Validation, Writing – review & editing. **Puyu Feng:** Conceptualization, Investigation, Validation, Visualization, Writing – review & editing. **Limin Duan:** Conceptualization, Funding acquisition, Investigation, Resources, Writing – review & editing. **Lijie Shi:** Data curation, Formal analysis, Validation. **Kai Ren:** Data curation, Investigation, Methodology. **Ning Yao:** Investigation, Software, Visualization. **Shang Chen:** Conceptualization, Methodology, Writing – review & editing. **Ke Liu:** Conceptualization, Investigation, Methodology, Validation, Visualization. **Matthew Tom Harrison:** Conceptualization, Investigation, Resources, Writing – review & editing. **Yi Li:** Data curation, Formal analysis, Resources. **De Li Liu:** Data curation, Formal analysis, Methodology, Resources. **Alfredo Huete:** Conceptualization, Investigation, Writing – review & editing. **Qiang Yu:** Conceptualization, Funding acquisition, Investigation, Resources, Writing – review & editing. **Guijun Yang:** Conceptualization, Funding acquisition, Resources, Validation, Writing – review & editing.

Declaration of competing interest

The authors declare the following financial interests/personal relationships which may be considered as potential competing interests: Qinsi He reports was provided by Inner Mongolia Agricultural University. If there are other authors, they declare that they have no known competing financial interests or personal relationships that could have appeared to influence the work reported in this paper.

Acknowledgments

This study was supported by the Inner Mongolia Autonomous Region Education Special Fund Project (2025), the National Natural Science Foundation of China (Grant Nos. 42501370, 42171303, and 42501067), the Open Research Fund of the National Key Laboratory of Soil and Water Conservation and Desertification Control (Grant No. Z2010025001-KJ2520), and the Natural Science Foundation of Inner Mongolia Autonomous Region of China (Grant No. 2024QN03070). The authors gratefully acknowledge Hushuai Nie for assistance with English language polishing.

Appendix A. Supplementary data

Supplementary data to this article can be found online at https://doi.org/10.1016/j.wace.2026.100924.

Data availability

No data was used for the research described in the article.

References

Allan, R.P., et al., 2020. Advances in understanding large-scale responses of the water cycle to climate change. Ann. N. Y. Acad. Sci. 1472 (1), 49–75.
Allen, R.G., Pereira, L.S., Raes, D., Smith, M., 1998. Crop evapotranspiration-guidelines for computing crop water requirements. FAO Irrigation and Drainage Paper 56. FAO, Roma, Italia.
Almazroui, M., et al., 2021. Assessment of CMIP6 performance and projected temperature and precipitation changes over South America. Earth Syst. Environ. 5 (2), 155–183.
Anderson, W., et al., 2023. Climate variability and simultaneous breadbasket yield shocks as observed in long-term yield records. Agric. For. Meteorol. 331.
Balting, D.F., AghaKouchak, A., Lohmann, G., Ionita, M., 2021. Northern Hemisphere drought risk in a warming climate. npj Clim. Atmos. Sci. 4 (1).
Borg, I., Groenen, P.J., 2005. Modern Multidimensional Scaling: Theory and Applications. Springer Science & Business Media.
Brunner, L., et al., 2020. Reduced global warming from CMIP6 projections when weighting models by performance and independence. Earth Syst. Dynam. 11 (4), 995–1012.
Chakraborti, R., et al., 2023. Crop switching for water sustainability in India's food bowl yields co-benefits for food security and farmers' profits. Nat. Water 1 (10), 864–878.
Chartrand, J., Pausata, F.S.R., 2020. Impacts of the North Atlantic Oscillation on winter precipitations and storm track variability in southeast Canada and the northeast United States. Weather Clim. Dyn. 1 (2), 731–744.
Chen, X., et al., 2022. Projected dry/wet regimes in China using SPEI under four SSP-RCPs based on statistically downscaled CMIP6 data. Int. J. Climatol. 42 (16), 9357–9384.
Chen, Z., et al., 2020. Global land monsoon precipitation changes in CMIP6 projections. Geophys. Res. Lett. 47 (14).
Chiang, F., Mazdiyasni, O., AghaKouchak, A., 2021. Evidence of anthropogenic impacts on global drought frequency, duration, and intensity. Nat. Commun. 12 (1), 2754.
Chou, C., Neelin, J.D., Chen, C.-A., Tu, J.-Y., 2009. Evaluating the "Rich-Get-Richer" mechanism in tropical precipitation change under global warming. J. Clim. 22 (8), 1982–2005.
Christidis, N., Stott, P.A., 2021. The influence of anthropogenic climate change on wet and dry summers in Europe. Sci Bull (Beijing) 66 (8), 813–823.
Ercin, E., Veldkamp, T.I.E., Hunink, J., 2021. Cross-border climate vulnerabilities of the European Union to drought. Nat. Commun. 12 (1), 3322.
Fernandez-Alvarez, J.C., et al., 2023. Projected changes in atmospheric moisture transport contributions associated with climate warming in the North Atlantic. Nat. Commun. 14 (1), 6476.
Flores, B.M., et al., 2024. Critical transitions in the Amazon forest system. Nature 626 (7999), 555–564.
Frierson, D.M.W., Scheff, J., 2015. Terrestrial aridity and its response to greenhouse warming across CMIP5 climate models. J. Clim. 28 (14), 5583–5600.
Galik, C.S., 2019. A continuing need to revisit BECCS and its potential. Nat. Clim. Change 10 (1), 2–3.
Gampe, D., et al., 2021. Increasing impact of warm droughts on northern ecosystem productivity over recent decades. Nat. Clim. Change 11 (9), 772–779.
Gaupp, F., Hall, J., Hochrainer-Stigler, S., Dadson, S., 2019. Changing risks of simultaneous global breadbasket failure. Nat. Clim. Change 10 (1), 54–57.
Greve, P., et al., 2014. Global assessment of trends in wetting and drying over land. Nat. Geosci. 7 (10), 716–721.

Greve, P., Roderick, M.L., Ukkola, A.M., Wada, Y., 2019. The aridity Index under global warming. Environ. Res. Lett. 14 (12).
Greve, P., Seneviratne, S.I., 2015. Assessment of future changes in water availability and aridity. Geophys. Res. Lett. 42 (13), 5493–5499.
Guo, L., et al., 2025. Developing a multivariate drought index to assess drought characteristics based on the SWAT-Copula method in the Poyang Lake basin, China. Ecol. Indic. 170.
Gurney, K.R., et al., 2022. Greenhouse gas emissions from global cities under SSP/RCP scenarios, 1990 to 2100. Glob. Environ. Change 73.
Hausfather, Z., Marvel, K., Schmidt, G.A., Nielsen-Gammon, J.W., Zelinka, M., 2022. Climate simulations: recognize the 'hot model'problem. Nature 605 (7908), 26–29.
He, Q., et al., 2022. Identifying effective agricultural management practices for climate change adaptation and mitigation: a win-win strategy in South-Eastern Australia. Agric. Syst. 203.
Held, I.M., Soden, B.J., 2006. Robust responses of the hydrological cycle to global warming. J. Clim. 19 (21), 5686–5699.
Huang, J., et al., 2023. Global climate impacts of land-surface and atmospheric processes over the Tibetan Plateau. Rev. Geophys. 61 (3).
Huang, J., Yu, H., Guan, X., Wang, G., Guo, R., 2015. Accelerated dryland expansion under climate change. Nat. Clim. Change 6 (2), 166–171.
IPCC, 2023. Summary for policymakers. In: Intergovernmental Panel on Climate, C. (Ed.), Climate Change 2021 – the Physical Science Basis: Working Group I Contribution to the Sixth Assessment Report of the Intergovernmental Panel on Climate Change. Cambridge University Press, Cambridge, pp. 3–32.
Ji, Y., Fu, J., Liu, B., Huang, Z., Tan, X., 2024. Uncertainty separation of drought projection in the 21st century using SMILEs and CMIP6. J. Hydrol. 628.
Jin, N., Shi, Y., Niu, W., He, L., 2023. Spatial and temporal patterns of agricultural drought in China during 1960–2020 characterized by use of the crop water deficit Abnormal Index. J. Hydrol. 627.
John, A., Douville, H., Ribes, A., Yiou, P., 2022. Quantifying CMIP6 model uncertainties in extreme precipitation projections. Weather Clim. Extrem. 36.
Jones, P.D., Jónsson, T., Wheeler, D., 1997. Extension to the North Atlantic Oscillation using early instrumental pressure observations from Gibraltar and south-west Iceland. Int. J. Climatol.: A Journal of the Royal Meteorological Society 17 (13), 1433–1450.
Kendall, M.G., 1975. Rank correlation methods. Griffin, London. J. Econom 13, 245–259.
Leng, G., Hall, J., 2019. Crop yield sensitivity of global major agricultural countries to droughts and the projected changes in the future. Sci. Total Environ. 654, 811–821.
Li, H., et al., 2021. Drylands face potential threat of robust drought in the CMIP6 SSPs scenarios. Environ. Res. Lett. 16 (11).
Li, L., et al., 2023a. The optimization of model ensemble composition and size can enhance the robustness of crop yield projections. Commun. Earth Environ. 4 (1).
Li, L., et al., 2023b. Integrating machine learning and environmental variables to constrain uncertainty in crop yield change projections under climate change. Eur. J. Agron. 149.
Liang, W., Zhang, M., 2022. Future changes of the Eddy moisture convergence in Winter over coastal lands in Eastern North America and East Asia. J. Geophys. Res. Atmos. 127 (17).
Liddicoat, S.K., et al., 2021. Compatible fossil fuel CO2 emissions in the CMIP6 Earth System models' historical and shared socioeconomic pathway experiments of the twenty-first century. J. Clim. 34 (8), 2853–2875.
Lobell, D.B., Deines, J.M., Tommaso, S.D., 2020. Changes in the drought sensitivity of US maize yields. Nat. Food 1 (11), 729–735.
Lu, J., Carbone, G.J., Grego, J.M., 2019. Uncertainty and hotspots in 21st century projections of agricultural drought from CMIP5 models. Sci. Rep. 9 (1), 4922.
Mann, H.B., 1945. Nonparametric tests against trend. Econometrica: J. Econom. Soc. 245–259.
McKenna, C.M., Maycock, A.C., 2021. Sources of uncertainty in Multimodel large ensemble projections of the Winter north Atlantic oscillation. Geophys. Res. Lett. 48 (14).
McPhaden, M.J., Zebiak, S.E., Glantz, M.H., 2006. ENSO as an integrating concept in earth science. Science 314 (5806), 1740–1745.
McSweeney, C.F., Jones, R.G., 2016. How representative is the spread of climate projections from the 5 CMIP5 GCMs used in ISI-MIP? Clim. Serv. 1, 24–29.
Meehl, G.A., et al., 2020. Context for interpreting equilibrium climate sensitivity and transient climate response from the CMIP6 Earth system models. Sci. Adv. 6 (26), eaba1981.
Mieno, T., Foster, T., Kakimoto, S., Brozović, N., 2024. Aquifer depletion exacerbates agricultural drought losses in the US High Plains. Nat. Water 2 (1), 41–51.
Minoli, S., Jagermeyr, J., Asseng, S., Urfels, A., Muller, C., 2022. Global crop yields can be lifted by timely adaptation of growing periods to climate change. Nat. Commun. 13 (1), 7079.
Morim, J., et al., 2019. Robustness and uncertainties in global multivariate wind-wave climate projections. Nat. Clim. Change 9 (9), 711–718.
Naumann, G., Cammalleri, C., Mentaschi, L., Feyen, L., 2021. Increased economic drought impacts in Europe with anthropogenic warming. Nat. Clim. Change 11 (6), 485–491.
Nicholson, S.E., 2013. The West African Sahel: a review of recent studies on the rainfall regime and its interannual variability. Int. Sch. Res. Not. 2013.
O'Neill, B.C., et al., 2016. The scenario model Intercomparison Project (ScenarioMIP) for CMIP6. Geosci. Model Dev. 9 (9), 3461–3482.
Parry, I.M., Ritchie, P.D.L., Cox, P.M., 2022. Evidence of localised Amazon rainforest dieback in CMIP6 models. Earth Syst. Dynam. 13 (4), 1667–1675.
Parsons, L.A., 2020. Implications of CMIP6 projected drying trends for 21st century Amazonian drought risk. Earths Future 8 (10).
Peng, L., Li, Y., Feng, H., 2017. The best alternative for estimating reference crop evapotranspiration in different sub-regions of mainland China. Sci. Rep. 7 (1), 5458.
Phelan, D.C., et al., 2018. Advancing a farmer decision support tool for agronomic decisions on rainfed and irrigated wheat cropping in Tasmania. Agric. Syst. 167, 113–124.
Pokhrel, Y., et al., 2021. Global terrestrial water storage and drought severity under climate change. Nat. Clim. Change 11 (3), 226–233.
Rivosecchi, A., Bollasina, M.A., Colfescu, I., 2024. Future changes in the influence of the NAO on Mediterranean winter precipitation extremes in the EC-Earth3 large Ensemble: the prominent role of internal variability. Atmos. Res. 304.
Ruane, A.C., McDermid, S.P., 2017. Selection of a representative subset of global climate models that captures the profile of regional changes for integrated climate impacts assessment. Earth Perspectives 4 (1).
Saji, N., Yamagata, T., 2003. Possible impacts of Indian Ocean dipole mode events on global climate. Clim. Res. 25 (2), 151–169.
Scafetta, N., 2022. Advanced testing of low, medium, and high ECS CMIP6 GCM simulations versus ERA5-T2m. Geophys. Res. Lett. 49 (6).
Sen, P.K., 1968. Estimates of the regression coefficient based on Kendall's tau. J. Am. Stat. Assoc. 63 (324), 1379–1389.
Shahpari, S., Allison, J., Harrison, M.T., Stanley, R., 2021. An integrated economic, environmental and social approach to agricultural land-use planning. Land 10 (4), 364.
Sheffield, J., Wood, E.F., Roderick, M.L., 2012. Little change in global drought over the past 60 years. Nature 491 (7424), 435–438.
Shi, H., et al., 2021. Terrestrial biodiversity threatened by increasing global aridity velocity under high-level warming. Proc. Natl. Acad. Sci. U. S. A. 118 (36).
Shi, L., Feng, P., Wang, B., Liu, D.L., Yu, Q., 2020. Quantifying future drought change and associated uncertainty in southeastern Australia with multiple potential evapotranspiration models. J. Hydrol. 590.
Singh, J., et al., 2022. Enhanced risk of concurrent regional droughts with increased ENSO variability and warming. Nat. Clim. Change 12 (2), 163–170.
Sándor, R., et al., 2023. Residual correlation and ensemble modelling to improve crop and grassland models. Environ. Model. Software 161, 105625.
Solazzo, E., Galmarini, S., 2015. A science-based use of ensembles of opportunities for assessment and scenario studies. Atmos. Chem. Phys. 15 (5), 2535–2544.
Stephenson, D.B., Pavan, V., Collins, M., Junge, M.M., Quadrelli, R., 2006. North Atlantic Oscillation response to transient greenhouse gas forcing and the impact on European winter climate: a CMIP2 multi-model assessment. Clim. Dyn. 27 (4), 401–420.
Thornthwaite, C.W., 1948. An approach toward a rational classification of climate. Geogr. Rev. 38 (1), 55–94.
Trabucco, A., Zomer, R.J., 2018. Global aridity index and potential evapotranspiration (ET0) climate database v2. CGIAR Consort Spat Inf 10, m9.
Ukkola, A.M., De Kauwe, M.G., Roderick, M.L., Abramowitz, G., Pitman, A.J., 2020. Robust future changes in meteorological drought in CMIP6 projections despite uncertainty in precipitation. Geophys. Res. Lett. 47 (11).
Vicente-Serrano, S.M., Beguería, S., López-Moreno, J.I., 2010. A multiscalar drought index sensitive to global warming: the standardized precipitation evapotranspiration index. J. Clim. 23 (7), 1696–1718.
Willett, P., 1988. Recent trends in hierarchic document clustering: a critical review. Inf. Process. Manag. 24 (5), 577–597.
Xiang, K., Li, Y., Horton, R., Feng, H., 2020. Similarity and difference of potential evapotranspiration and reference crop evapotranspiration – a review. Agric. Water Manag. 232.
Xie, W., et al., 2023, 616, 300–305. Crop switching can enhance environmental sustainability and farmer incomes in China. Nature.
Xiong, J., Guo, S., Chen, J., Yin, J., 2022. Global evaluation of the "dry gets drier, and wet gets wetter" paradigm from a terrestrial water storage change perspective. Hydrol. Earth Syst. Sci. 26 (24), 6457–6476.
Xu, C., et al., 2019. Increasing impacts of extreme droughts on vegetation productivity under climate change. Nat. Clim. Change 9 (12), 948–953.
Xu, L., Chen, N., Yang, C., Zhang, C., Yu, H., 2021. A parametric multivariate drought index for drought monitoring and assessment under climate change. Agric. For. Meteorol. 310.
Xu, P., et al., 2024, 626, 792–798. Fertilizer management for global ammonia emission reduction. Nature.
Xu, S., et al., 2022. Delayed use of bioenergy crops might threaten climate and food security. Nature 609 (7926), 299–306.
Yao, N., et al., 2019. Influence of the accuracy of reference crop evapotranspiration on drought monitoring using standardized precipitation evapotranspiration index in mainland China. Land Degrad. Dev. 31 (2), 266–282.
Yao, N., et al., 2020. Projections of drought characteristics in China based on a standardized precipitation and evapotranspiration index and multiple GCMs. Sci. Total Environ. 704, 135245.
Yao, N., Li, Y., Lei, T., Peng, L., 2018. Drought evolution, severity and trends in mainland China over 1961–2013. Sci. Total Environ. 616–617, 73–89.
Yao, Z., et al., 2024. A global meta-analysis of yield-scaled N(2) O emissions and its mitigation efforts for maize, wheat, and rice. Glob. Change Biol. 30 (2), e17177.
Yazdandoost, F., Moradian, S., Izadi, A., Aghakouchak, A., 2021. Evaluation of CMIP6 precipitation simulations across different climatic zones: uncertainty and model intercomparison. Atmos. Res. 250.
Zabel, F., et al., 2021, 27: 3870-3882. Large potential for crop production adaptation depends on available future varieties. Glob. Change Biol.
Zaitchik, B.F., Rodell, M., Biasutti, M., Seneviratne, S.I., 2023. Wetting and drying trends under climate change. Nat. Water 1 (6), 502–513.
Zhang, G., et al., 2020. Response of Tibetan Plateau lakes to climate change: trends, patterns, and mechanisms. Earth Sci. Rev. 208.

Zhang, G., Nan, Z., Zhao, L., Liang, Y., Cheng, G., 2021a. Qinghai-Tibet Plateau wetting reduces permafrost thermal responses to climate warming. Earth Planet Sci. Lett. 562.
Zhang, Q., et al., 2022. High sensitivity of compound drought and heatwave events to global warming in the future. Earths Future 10 (11).
Zhang, Y., et al., 2023. Southern Hemisphere dominates recent decline in global water availability. Science 382 (6670), 579–584.
Zhang, Y., Keenan, T.F., Zhou, S., 2021b. Exacerbated drought impacts on global ecosystems due to structural overshoot. Nat. Ecol. Evol. 5 (11), 1490–1498.
Zheng, H., et al., 2024. Projections of future streamflow for Australia informed by CMIP6 and previous generations of global climate models. J. Hydrol. 636.
Zhou, S., et al., 2022. Large divergence in tropical hydrological projections caused by model spread in vegetation responses to elevated CO2. Earths Future 10 (4).